ACS APPLIED MATERIALS & INTERFACES

Research Article

www.acsami.org

Highly Electrically Conducting Glass-Graphene Nanoplatelets Hybrid Coatings

E. Garcia,[†] A. Nistal,[†] A. Khalifa,[‡] Y. Essa,[‡] F. Martín de la Escalera,[‡] M. I. Osendi,[†] and P. Miranzo*[,†]

[†]Institute of Ceramics and Glass (ICV-CSIC), Kelsen 5, 28049 Madrid, Spain

[‡]Aernnova Engineering Solutions Ibérica, Av. de Manoteras 20, 28050 Madrid, Spain

Supporting Information

ABSTRACT: Hybrid coatings consisting of a heat resistant Y_2O_3–Al_2O_3–SiO_2 (YAS) glass containing 2.3 wt % of graphene nanoplatelets (GNPs) were developed by flame spraying homogeneous ceramic powders-GNP granules. Around 40% of the GNPs survived the high spraying temperatures and were distributed along the splat-interfaces, forming a percolated network. These YAS-GNP coatings are potentially interesting in thermal protection systems and electromagnetic interference shields for aerospace applications; therefore silicon carbide (SiC) materials at the forefront of those applications were employed as substrates. Whereas the YAS coatings are nonconductive, the YAS-GNP coatings showed in-plane electrical conductivity (~10^2 S·m^{-1}) for which a low percolation limit (below 3.6 vol %) is inferred. Indentation tests revealed the formation of a highly damaged indentation zone showing multiple shear displacements between adjacent splats probably favored by the graphene sheets location. The indentation radial cracks typically found in brittle glass coatings are not detected in the hybrid coatings that are also more compliant.

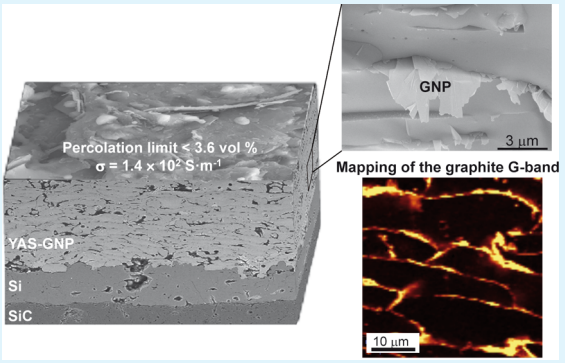

KEYWORDS: *hybrid coatings, graphene nanoplatelets, heat resistant glass, thermal spraying, electrical conductivity, strain tolerance, electromagnetic interference shielding, thermal protection*

INTRODUCTION

High-temperature composites used for aeronautics and aerospace applications consist chiefly of carbon or silicon carbide matrices reinforced with either carbon or silicon carbide fibers.[1,2] These composites may experience corrosion and oxidation damages because of the severe operating conditions of temperature and atmosphere. Therefore, research on new lightweight protecting coatings is a main concern for those sectors, also involved in the shielding against external events like lightning strike damage and electromagnetic interference (EMI).[2−4] A novel trend in this field is denoted by the development of multifunctional hybrid coatings with multiscale architectures.[5−7] In this context, coatings containing graphene fillers (GFs) are progressively investigated presuming similar improvements, in electrical, thermal, tribological, and mechanical properties, to those observed in bulk composites.[8,9] Some glass-ceramic compositions are promising for effective high temperature protection of engineering components against corrosion/oxidation with additional self-healing capabilities.[10] Hence, the addition of GFs to those glass-ceramics could improve the system performance by developing extra electrical and thermal functionalities.

Thermal spraying techniques are industrially implemented cost-effective coating methods based on heating and accelerating the source material toward the substrate.[11] However, research on ceramic/GF hybrid coatings is quite limited, probably owing to the high processing temperatures normally involved in thermal spraying techniques that could bring doubts about GFs damage. The few works[12−14] reporting ceramic/GF coatings processed by thermal spraying methods are mostly focused on wear and biocompatibility issues. To the best of the authors' knowledge, there is not any work on thermal sprayed glass-ceramic/GFs coatings intended for protection of high-temperature aerospace components. In a recent work by some of the present authors, flame spraying (FS) was applied to achieve high melting temperature Y_2O_3–Al_2O_3–SiO_2 (YAS) glass coatings[15] that could be effective in thermal protection systems (TPS). Presently, the feasibility of the flame spraying method to coat SiC substrates using YAS-graphene nanoplatelets (GNPs) granules is demonstrated. The distribution and possible degradation of the GNPs is monitored during the whole process by scanning electron microscopy (SEM) and μ-Raman spectroscopy; furthermore, the thermal and electrical conductivities of the coating are determined and compared to the GNPs-free YAS coating. The prospects of a thermally resistant glass-ceramic/GF hybrid coating attached onto a silicon carbide substrate exhibiting new functionalities, such as enhanced electrical conductivity are demonstrated in this work.

Received: March 23, 2015
Accepted: July 29, 2015
Published: July 29, 2015

DOI: 10.1021/acsami.5b02553
ACS Appl. Mater. Interfaces 2015, 7, 17656−17662

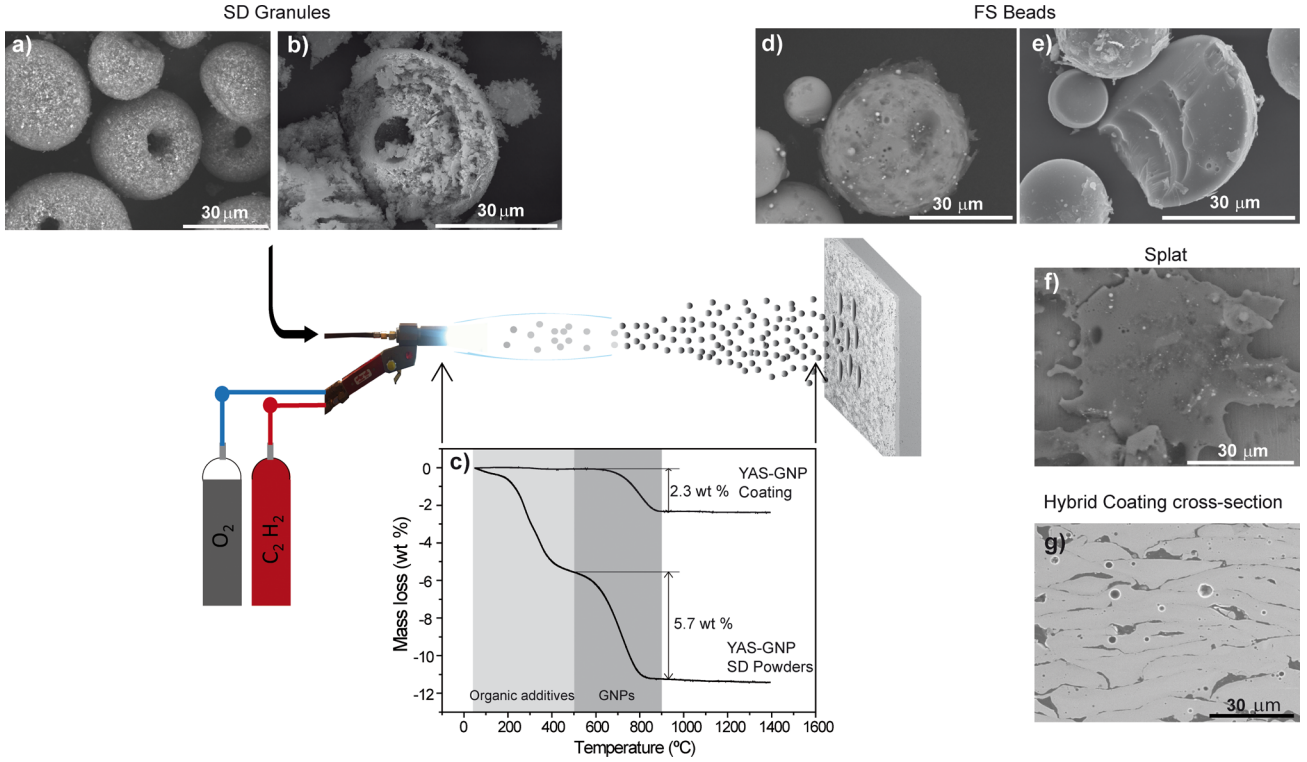

Figure 1. Schematic illustrations of the flame spraying process for the YAS-GNP coating formation including SEM micrographs of the original YAS-GNP granules (a and b), the FS droplets after quenching in liquid N_2 (d and e), a single splat spread over a flat surface (f), and the microstructure of the obtained coating in a polished cross-section (g). The thermogravimetric analysis of the YAS-GNP granules and the hybrid coating is depicted in (c).

RESULTS AND DISCUSION

The schematic description of the YAS-GNP coating procedure is displayed in Figure 1. The feedstock is formed by granules YAS containing 6.5 wt % GNPs (Figures 1a and 1b) fabricated by spray drying (SD), and consists of spherical shaped particles of ∼30 μm formed by compacted powders enclosing GNPs. The GNPs show a circular arrangement (Figure 1b) that is probably linked to the dragging effect caused by the water ejecting from the atomized droplet and the droplet rotation induced by the hot air stream throughout the spray drying process.[16]

The thermogravimetric (TG) analysis (Figure 1c) of the YAS-GNP granules reveals that weight losses occur in two different temperature regimes: the first, between 100 and 500 °C, of about 5% is due to residual water evaporation and burning out of organic additives employed for homogenization and stabilization of the suspension for the spray drying process (e.g., residues of either polyelectrolyte, gum arabic, or binder); and the second, from 500 to 900 °C, amounting to 5.7% of further weight loss due to the GNPs combustion.

The SEM observation of YAS-GNP beads, obtained by projecting the FS molten droplets into liquid N_2, helps to visualize the transformations occurring in the sprayed particles just before impacting on the substrate. The YAS-GNP beads (Figure 1d and 1e) show high compactness and the existence of scattered dark spots on the bead surface that occasionally emerge as subtle veils (Figure 1d). These dark features are not detected inside the particles (Figure 1e). On the whole, these observations suggest a poor wettability of GNPs by the liquid formed in the course of the spraying process. This GNP low wettability together with a buoyancy effect because of their inferior density (<2.20 g·cm^{-3}), as compared to the typical of a YAS glass (3.51 g·cm^{-3}),[15] probably produced their expelling toward the droplet surface all along the particle flight toward the blank. Hence, when droplets impinge onto the substrate and rapidly cool down and spread (Figure 1f), GNPs become trapped between successive splats as the microstructure of the YAS-GNP coating in cross-section view reveals (Figure 1g), representing well-defined splats flanked by darker features. TG analysis of the YAS-GNP coating (Figure 1c) shows no signs of organic additives, that is, no weight loss is detected below 500 °C, thus indicating they have burned during thermal spraying; consequently, the 2.3% weight loss occurring between 500 and 900 °C is due to the combustion of the GNPs remaining in the coating. This figure is about 40% of the weight loss detected in the feedstock for the same temperature interval, and represents the GNP yield after the FS process. The X-ray diffraction (XRD) pattern obtained from the top surface of the hybrid coating (Figure S1 in the Supporting Information, SI) evidence the occurrence of the (003) diffraction peak of graphite and the presence of an amorphous bump.

Despite the fact that the O_2/C_2H_2 combustion takes place in air atmosphere and involves gas temperatures above 3000 °C,[17] the given thermal spraying conditions involved very short particle flying times (∼2 ms) that probably produced thermal gradients in the granules, the interior being at lower temperature than the surface. Both the short time and the temperature gradient facilitate the GNPs survival, provided that there is a good dispersion of the GNPs within the granules. In this way, although the GNPs at the surface would burn rapidly, those inside the granule would be initially protected by the surrounding semimolten mass. Eventually, GNPs would migrate to the droplet surface once YAS melting occurs but,

DOI: 10.1021/acsami.5b02553
ACS Appl. Mater. Interfaces 2015, 7, 17656−17662

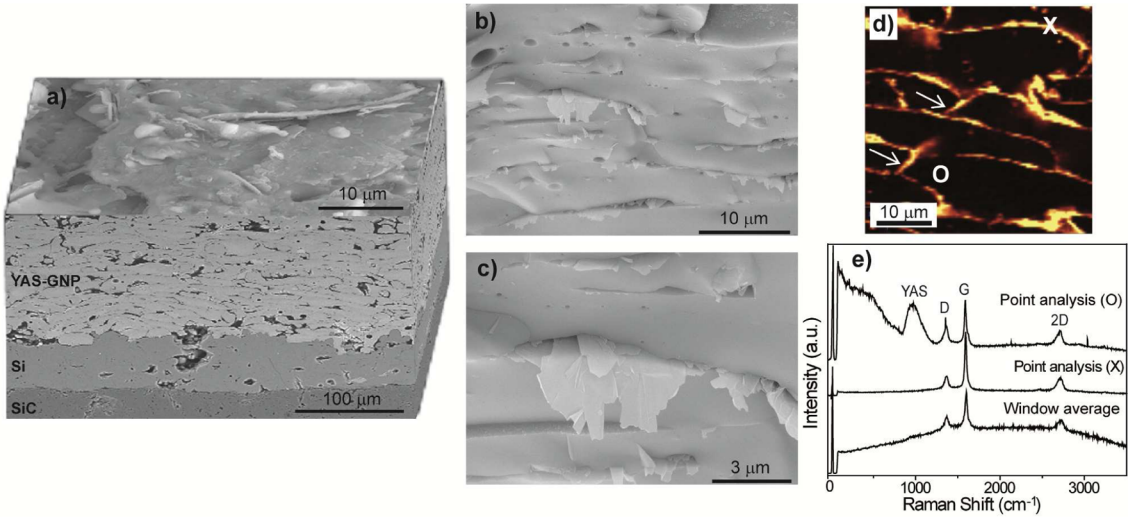

Figure 2. Microstructure of the YAS-GNP hybrid coating: (a) assembly of SEM images of the top and cross-section surfaces also showing the silicon bond coat and the SiC substrate; (b, c) SEM micrographs of the coating fracture surface at different magnification; (d) false colored image built by filtering the I_G signal of the Raman spectra mapping an area of 45 μm × 45 μm of the hybrid coating cross-section; (e) plots of average Raman spectrum of the mapped area and the point Raman spectra of X and O spots marked in panel d. Acquisition time of 30 s was used for the point spectrum of the YAS matrix. White arrows in panel d point to GNPs misoriented from the horizontal axis.

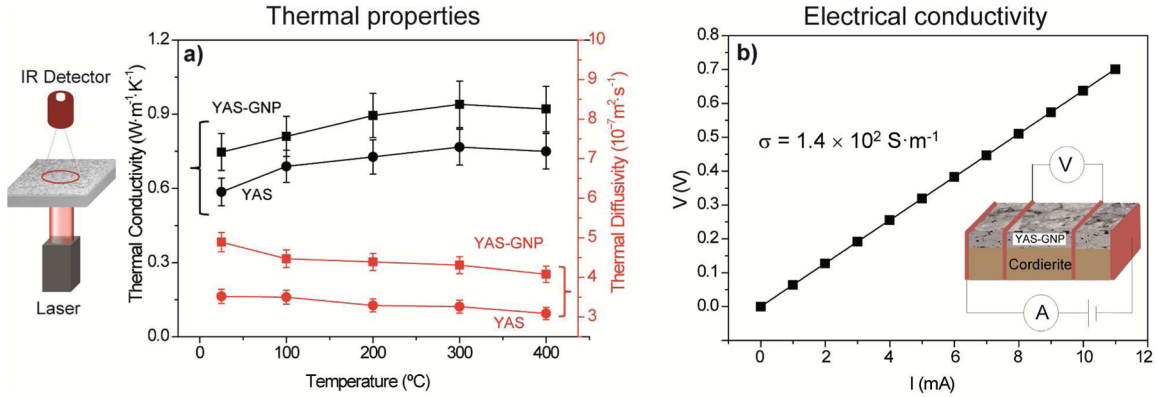

Figure 3. (a) Thermal diffusivity and conductivity values of YAS and YAS-GNP coatings determined in the through-thickness direction by the laser flash technique for the 25−400 °C temperature range. (b) *V*−*I* curve obtained from DC measurements, using the four probe method, at room temperature for the YAS-GNP/cordierite system.

as it seems, the kinetics of the whole process is fast enough to avoid their complete depletion. The presence of GNPs in the coating justifies the black color of the YAS-GNP coating (see Figure S1).

As seen in Figure 2a, the flame sprayed YAS-GNP hybrid coating has the usual *splat* structure, shows continuity and good adherence to the Si bond coat, firmly attached to the SiC substrate as well. The average thickness of the hybrid coating is 169 ± 10 μm, quite close to that of the GNPs-free YAS coating (197 ± 19 μm) and around 3 times thicker than the breadth of the Si bond layer (56 ± 10 μm).

Both YAS and YAS-GNP coatings reach similar densities (80% and 76% of the corresponding theoretical densities), but show some significant microstructural differences; in particular, the distinctive elongated dark features between the flattened lamellas perceived in the cross section view of the YAS-GNP coating (Figure 2a). These features are different from the residual spherical pores observed in the plain YAS coating (see Figure S1) and are clearly identified as nanoplatelets in the fracture surface images of the YAS-GNP coating (Figures 2b and 2c), where GNPs appear pulling out from the interfaces between lamellas. Furthermore, GNPs seem to be mostly oriented in a parallel manner to the coating surface although the top coating image (Figure 2a) also reveals the existence of some nanoplatelets protruding from the coating.

The D- (~1360 cm^{-1}), G- (~1595 cm^{-1}), and 2D- (~2717 cm^{-1}) characteristic Raman bands of graphitic structures[18] are clearly observed in the Raman spectra (Figure 2e) acquired on the cross-section of the YAS-GNP hybrid coating by mapping a 45 μm × 45 μm area. The Raman intensity image built by filtering the G-band signal clearly confirms the existence of a continuous network of GNPs occupying the intersplat spaces (Figure 2d). The intense background observed in the average spectrum (Figure 2e), not present in the point spectra of GNP regions (X mark in Figure 2d), is a fluorescence effect due to the presence of some porosity and the interfaces. The intensity ratio between D- and G-peaks (I_D/I_G) for the YAS-GNP average Raman spectrum increases when compared to that for the original GNPs (shown in Figure S2) from 0.10 to 0.35, which could be ascribed to a higher contribution of the defective GNP edges when analyzing the coating cross-section. An even higher I_D/I_G ratio of 0.38 was calculated for point

DOI: 10.1021/acsami.5b02553
ACS Appl. Mater. Interfaces 2015, 7, 17656−17662

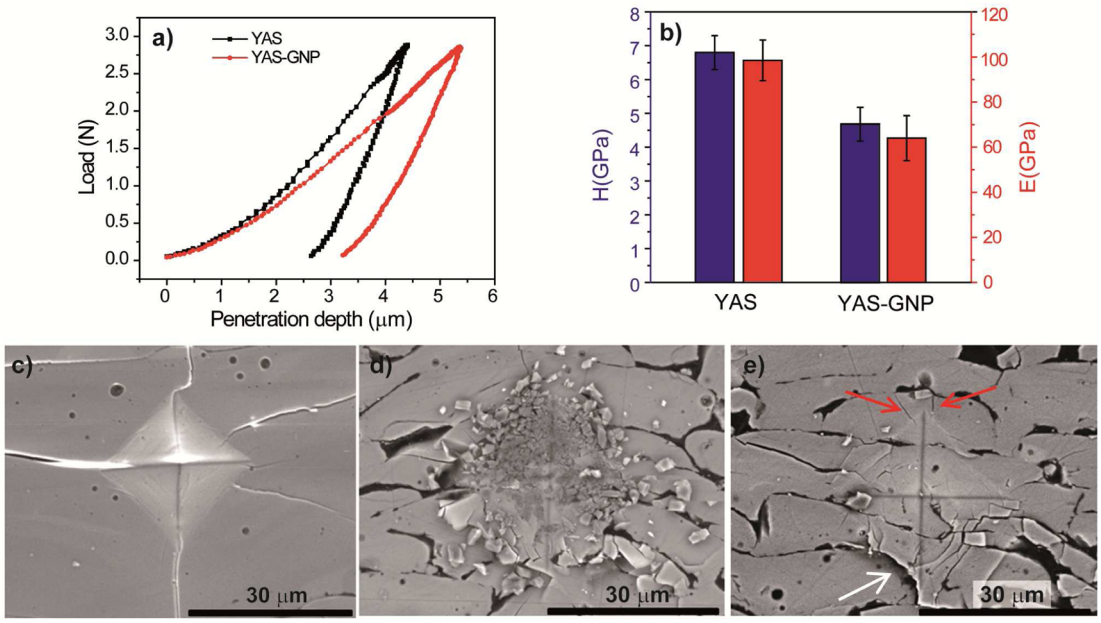

Figure 4. Vickers indentation tests at a load of 2.9 N done on the cross sections of the YAS and YAS-GNP hybrid coatings: (a) examples of indentation load versus penetration depth curves; (b) hardness (H) and elastic modulus (E); and SEM micrographs showing typical indentations imprints for YAS (c) and YAS-GNP (d and e) coatings. White and red arrows in panel e point to material pull-out and crack arresting at GNP interfaces, respectively.

spectra recorded at regions of maximum G-band intensity (X in Figure 2d).

When analyzing the Raman spectrum of YAS matrix regions (O marks in Figure 2d and 2e), the band at ~950 cm^{-1} previously ascribed to the aluminosilicate glassy phase[19] is clearly observed. Conversely, the same band is not detected in the window averaged spectrum because the high Raman scattering efficiency of GNPs masks any other signals.

The thermal diffusivity (α) and conductivity (κ) of the coatings (Figure 3a) were calculated using a three-layer model[20] from the apparent through-thickness thermal diffusivity (α_{app}) measured for the "coating/bond-coat/substrate" systems. The α and κ values of YAS were very low and almost constant with temperature, $(3.5-3.1) \times 10^{-7}$ $m^2 \cdot s^{-1}$ and 0.59–0.75 $W \cdot m^{-1} \cdot K^{-1}$, respectively, in the 25–400 °C temperature range, which are common values for glassy and amorphous materials. The room temperature α (4.9×10^{-7} $m^2 \cdot s^{-1}$) and κ (0.75 $W \cdot m^{-1} \cdot K^{-1}$) values for YAS-GNP coatings are ~60 and 30% higher, respectively, than that for the YAS coating alone. The increase of the through-thickness thermal conductivity differs from data reported in bulk GNP/Si_3N_4 composites, where the in-plane thermal conductivity increased with the GNP content but the through-thickness decreased due to the existence of thermal resistances.[21] In those composites, preferential orientation of GNPs occurs by the alignment of their *basal* plane perpendicular to the loading axis of the spark plasma sintering furnace. However, for the present coatings, the GNPs essentially fill the intersplats gaps (Figure 2), therefore, reducing the thermal resistance associated with the intersplats boundaries common in thermally sprayed coatings.[22−24] Besides, some effect of misorientation of the GNP plane from the horizontal axis actually occurs (see white arrows in Figure 2d), thus multiplying the number of GNP-GNP contacts, with lower thermal resistance than the GNP-matrix contacts, in the direction perpendicular to the coating surface, contributing in this way to the observed enhancement of the through-thickness thermal conductivity. The in-plane apparent thermal diffusivity at room temperature (see Figure S3) of the whole YAS-GNP/Si/SiC system also increases ($3.08 \pm 0.03 \times 10^{-5}$ $m \cdot s^{-1}$) compared to YAS/Si/SiC system ($2.35 \pm 0.05 \times 10^{-5}$ $m \cdot s^{-1}$), as expected. Consequently, the creation of a connected GNPs network in the coating slightly increases heat conduction in both directions. However, a high thermal conductivity is not the main requirement of surface coating for high temperature reusable insulation tiles used in TPS.[25] Actually, high emissivity and corrosion resistance are basic issues. In fact, the previously used black borosilicate glass coatings[25] have typical thermal conductivity of 1.1 $W \cdot m \cdot K^{-1}$. The black color of the GNP-YAS coating certainly forecasts a good behavior in TPS.

The electrical conductivity (σ) at room temperature of the YAS-GNP coating was measured on specimens directly projected over an insulator cordierite ($2MgO \cdot 2Al_2O_3 \cdot 5SiO_2$) substrate. In the case of the YAS/cordierite system, σ was below the experimental detection limit ($<10^{-13}$ S m^{-1}) whereas for the YAS-GNP/cordierite system a linear $V-I$ response was observed in the whole measurement range (Figure 3b), with an electrical conductivity of 1.4×10^2 $S \cdot m^{-1}$, that is, 15 orders of magnitude above that of the GNPs-free YAS coating. These data indicate that GNPs form a connected network through the entire coating allowing the current flow across the GNP-GNP contacts. Therefore, the percolation limit for electrical conduction in these composite coatings should be below 3.6 vol %, which is in the low boundary of percolation limits reported for most graphene/ceramic bulks and films as well (~3–8 vol %).[26−30] Additionally, σ of this hybrid coating is among the highest reported for GNP/ceramic composites with similar volume fractions of graphene fillers (σ of $0.4-1.8 \times 10^2$ $S \cdot m^{-1}$),[29−32] with the only exception of a work on rGO/Al_2O_3 composites processed by sol–gel methods reporting a topmost value of 10^3 $S \cdot m^{-1}$ and a percolation limit of 0.38 vol %.[33] If the comparison is restricted to coatings and films, the conductivity

DOI: 10.1021/acsami.5b02553
ACS Appl. Mater. Interfaces 2015, 7, 17656−17662

of the present hybrid coatings is 4 orders of magnitude higher than that of graphene/SiO_2 thin films (8×10^{-2} S·m^{-1}) with similar proportions of graphene.[28] The extraordinary electrical conductivity achieved for the YAS-GNP hybrid coatings envisages promising applications, like EMI shielding at high temperature.

Vickers indentation tests for the YAS-GNP coating show higher penetration depth (~21% increase) and permanent deformation (~22%) as compared to the YAS coating, for equal loads (Figure 4a). In the same sense, H data, depicted in Figure 4b, confirm that the YAS-GNP hybrid coating has about 30% lower hardness (4.7 ± 0.5 GPa) than the YAS coating. Similar trend is found for E as it decreases from 98 ± 9 GPa for the YAS coating to 64 ± 10 GPa for the YAS-GNP (35% lower). Parallel declining trend on hardness and elastic modulus has been reported for bulk ceramic and glass systems by adding graphene nanostructures.[34,35] For present coatings, the location of GNP at the intersplat boundaries and the feeble attachment to the surrounding matrix (Figure 2) could favor easy shear at these boundaries. This effect is not necessarily detrimental as it increases the deformability of these coatings which would improve their strain tolerance.

Finally, as shown in Figure 4d and 4e, the indentation imprints for the YAS-GNP hybrid coating show quite different features from those observed for the YAS coating (Figure 4c). First, radial cracks emanating from the indentation corners, which are typically generated in the brittle YAS coating (Figure 4c), are not developed in the YAS-GNP coating (Figure 4d and 4e); instead a highly damaged indentation zone showing material pull-out is perceived in some cases (Figure 4d), while other indentation imprints exhibit signs of certain shear displacement between adjacent splats (white arrow in Figure 4e). All these effects are compatible with the occurrence of weak interfaces at the intersplat boundaries where graphene sheets are situated. It is recognized that a "weak" interface in brittle matrix composites has a fracture energy which satisfies debonding requirements in the presence of matrix-fiber cracks.[36] The propagation of cracks is then subjected to mode mixity, debonding and large-scale bridging. Consequently, there is an increased toughness dominated by frictional dissipation at sliding interfaces, coupled with the effects of the large-scale bridging and pull-out phenomena. Under the complex indentation stress field, sliding at these weak interfaces and also dissipative friction effects are plausible, thus dissipating energy and reducing main crack propagation. The observed indentation imprint features point toward an enhancement of the coating toughness due to the presence of GNPs. In fact, in cases where small indentation median cracks generated at the imprint corners (see red arrows in Figure 4e), they are always arrested when reaching GNPs. The observed differences between indentation imprints (Figure 4d,e) are due to several effects as the large lateral dimensions of the splats (>30 μm) that form the coating and the GNPs location at the intersplat boundaries. As a consequence of the reduced size of the coating, the use of high indentation loads was avoided; for low loads, the corresponding indentation volume is small compared to the characteristic microstructural feature size, and then, the developed stress field strongly depends on the point where load is applied, that is, center of a splat, intersplat boundary or a triple point, explaining the different indentation features shown in Figure 4d and e. In any case, for H and E estimations only well-developed indentations as that of Figure 4e were considered.

CONCLUSIONS

A thick glass-graphene hybrid coating of ~170 μm was successfully produced by flame spraying an in-house processed feedstock over a silicon carbide substrate. The homogeneous mixture of the Y_2O_3–Al_2O_3–SiO_2 ceramic composition and the graphene nanoplatelets inside the feedstock granules assured the GNP survival in the hybrid coating in spite of the high temperatures and oxidative environment of the flame spraying process. The developed coating contains 3.6 vol % of highly crystalline and oriented GNPs located at the intersplat sites forming a percolated network. Accordingly, this coating shows extraordinary high electrical conductivity (1.4×10^2 S·m^{-1}) as compared to the insulating GNPs-free coating. The hybrid coating also shows increased thermal conductivity (30%). The indentation imprints show strong interactions with the coating microstructure, where GNPs preclude the crack advance. The reduced elastic modulus of this hybrid material helps to increase the compliance and improve the strain tolerance of these coatings. All these properties, combined with the self-healing capability of the matrix, open new prospects for innovative applications of these hybrid coatings like TPS or EMI protection in aerospace applications.

EXPERIMENTAL SECTION

The YAS composition $17.5Y_2O_3$–$29.5Al_2O_3$–$53.0SiO_2$ (in mol %) was selected because of its glass formation ability and its thermal expansion coefficient close to that of the SiC substrates.[15,37] High purity powders (>99.5%) were employed for preparing the glass composition, in particular Y_2O_3 (H.C. Starck, Germany), Al_2O_3 (SM8, Baikowski, France), and SiO_2 (Alfa Aesar, Germany). Commercially available GNPs (N008-100-P-10, Angstron Materials Inc., U.S.) with nominal length between 5–10 μm and thickness of 50–100 nm were used as filler in a concentration of 10 vol % (6.5 wt %). The YAS powders were homogeneously mixed by attrition milling for 1.5 h in water with 0.4 wt % of a polyelectrolyte dispersant (Dolapix CE 64 CA, Zschimmer- Schwarz, Lahnstein, Germany). Meanwhile, a stable suspension of GNPs in water with 4 wt % gum arabic (Sigma-Aldrich, U.S.) was prepared in an ultrasonic bath (100 W, 50/60 Hz, J. P. Selecta Ultrasons, Spain) for 30 min. Both GNP and YAS suspensions were jointly attrition milled for 30 min. The suspension was freeze-dried[38] to avoid the segregation of the different constituents. YAS-GNP hybrid granules with the adequate size distribution and morphology for the flame spray process were obtained by spray drying using a 50 wt % solids content water suspension of the powders mixture and adding a 5 wt % of binder (Optapix PS 94, Zschimmer-Schwarz, Germany).[38] A similar process was used for preparing the plain YAS feedstock. The SD powders were flame sprayed onto conditioned SiC and cordierite substrates (see Figures S4 and S5) using an oxyacetylene gun (CastoDyn DS 8000, Castolin-Eutectic, Spain) with a gas mixture of O_2/C_2H_2 in the ratio of 33/24 SLPM (standard liters per minute) and a stand-off distance of 14 cm. Similarly, the YAS-GNP powders were FS into a metal container filled with liquid N_2 for attaining flame spheroidized beads.[39] These beads helped to understand changes occurring in the YAS-GNP granules throughout the spraying process.

Weight loss up to 1400 °C of the YAS-GNP granules and the corresponding powdered freestanding coating were recorded by TG analysis (STA 409 Netzsch, Germany) in air at a heating rate of 10 °C·min^{-1} to have an appraisal of the GNPs content in each stage of the preparation process.

Densities (ρ) of 2.80 and 2.56 g·cm^{-3} were measured on YAS and YAS-GNP freestanding samples by the water immersion method, which gives relative densities of 80 and 76% of the theoretical value, respectively, calculated considering the densities of the YAS glass[15] (3.51 g·cm^{-3}) and the GNPs (2.20 g·cm^{-3}).

The microstructure of SD granules, FS beads and coatings was examined on the fracture surface, upper surface and polished cross

DOI: 10.1021/acsami.5b02553
ACS Appl. Mater. Interfaces 2015, 7, 17656–17662

section with both table-top SEM (TM1000, Hitachi, Japan) and FE-SEM (S-4700 Hitachi, Japan). Raman spectra were recorded from cross-sectioned polished coatings at room temperature using a confocal μ-Raman imaging system (Alpha 300 WITec GmbH, Germany) with a laser excitation wavelength of 532 nm. Raman maps of 150 × 150 pixels, recording one spectrum per pixel and using 60 ms of acquisition time, were recorded on 45 μm × 45 μm scanned areas of the hybrid coating.

YAS/Si/SiC and YAS-GNP/Si/SiC square specimens with lateral dimensions of 8.8 and 20 mm were used for measuring apparent through-thickness and in-plane thermal diffusivity, respectively, by the laser-flash method (Thermaflash 2200, Holometrix/Netzsch, U.S.). The total thickness of both types of specimens was 0.86 mm; the top glass coating with thickness ~0.20 mm, the Si bond coat with ~0.06 mm and the SiC substrate with ~0.6 mm. The samples where coated with colloidal graphite to enhance absorption of the laser beam. The through-thickness α_{app} measurements were done in Ar atmosphere from 25 to 400 °C. From the α_{app} values, and considering reported thermal properties for SiC and Si,[40] the thermal diffusivity and conductivity of the coatings were calculated using the analytical model for heat diffusion in three layered systems[20] and iterative software routines. The measured density and the specific heat (C_p) estimated by the rule of mixtures using thermodynamic data[41] were used in the calculations. In-plane α_{app} of the systems was measured at room temperature using a distinct setup (see Figure S3) and a two-dimensional model[42] for analyzing the recorded temperature rise. Data were averaged over at least 5 measurements.

DC electrical conductivity was measured using the four-probe method on samples with dimensions 15.5 × 5.5 × 3.0 mm^3 machined from the YAS and the YAS-GNP hybrid coatings directly sprayed over insulating cordierite substrates (see Figure S5). Pt wires were attached to the lateral surfaces of the coating/cordierite system using Ag paste. An Autolab potentiostat/galvanostat (Autolab PGSTAT 302N, Eco Chemie, The Netherlands) was employed in galvanostatic configuration for assuring a fixed DC current. The voltage drop was recorded at two inner Pt electrodes separated by a distance of 5 mm. The resistance of the system was calculated from the slope of the $V-I$ curve. As cordierite is a dielectric material, the conductivity was deduced considering as effective conducting area that of the coating cross section, that is, ~0.12 × 3 mm^2 (configuration shown in Figure 3b).

Elastic modulus and hardness were evaluated on the polished cross sections of the coatings by instrumented Vickers indentation (ZHU 2.5; Zwick GmbH & Co. KG, Germany), which simultaneously records load and indentation depth. The elastic modulus of the material was calculated according to the Oliver–Pharr method[43] from the reduced modulus. At least 10 measurements at a load of 2.9 N, applied for 5 s, were completed for each sample. The indentation imprints were analyzed by FE-SEM.

■ ASSOCIATED CONTENT

Supporting Information

The Supporting Information is available free of charge on the ACS Publications website at DOI: 10.1021/acsami.5b02553.

Microstructure and crystalline phase analysis on YAS and YAS-GNP coatings, SEM and Raman spectrum of the original GNPs, in-plane thermal diffusivity measurement setup, and information about conditioning of SiC substrates and fabrication of the cordierite substrates (PDF)

■ AUTHOR INFORMATION

Corresponding Author

*E-mail: pmiranzo@icv.csic.es.

Author Contributions

The manuscript was written through contributions of all authors. All authors have given approval to the final version of the manuscript. All authors contributed equally.

Notes

The authors declare no competing financial interest.

■ ACKNOWLEDGMENTS

This work was supported by the Spanish Ministry of Economy and Competitiveness (MINECO) under project INNPACTO IPT-2012-0800-420000. Experimental support of Dr. D. Pérez-Coll in the measurement of DC electrical conductivity is greatly acknowledged.

■ REFERENCES

(1) Krenkel, W.; Berndt, F. C/C–SiC Composites for Space Applications and Advanced Friction Systems. *Mater. Sci. Eng., A* **2005**, *412*, 177–181.

(2) Spitsberg, I.; Steibel, J. Thermal and Environmental Barrier Coatings for SiC/SiC CMCs in Aircraft Engine Applications. *Int. J. Appl. Ceram. Technol.* **2004**, *1*, 291–301.

(3) Gagné, M.; Therriault, D. Lightning Strike Protection of Composites. *Prog. Aerosp. Sci.* **2014**, *64*, 1–16.

(4) Albano, M.; Micheli, D.; Gradoni, G.; Morles, R. B.; Marchetti, M.; Moglie, F.; Mariani Primiani, V. Electromagnetic Shielding of Thermal Protection System for Hypersonic Vehicles. *Acta Astronaut.* **2013**, *87*, 30–39.

(5) Sanchez, C.; Julián, B.; Belleville, P.; Popall, M. Applications of Hybrid Organic–Inorganic Nanocomposites. *J. Mater. Chem.* **2005**, *15*, 3559–3592.

(6) Pagliaro, M.; Ciriminna, R.; Palmisano, G. Silica-based Hybrid Coatings. *J. Mater. Chem.* **2009**, *19*, 3116–3126.

(7) Nicole, L.; Laberty-Robert, C.; Rozes, L.; Sanchez, C. Hybrid Materials Science: a Promised Land for the Integrative Design of Multifunctional Materials. *Nanoscale* **2014**, *6*, 6267–6292.

(8) Kuilla, T.; Bhadra, S.; Yao, D.; Kim, N. H.; Bose, S.; Lee, J. H. Recent Advances in Graphene based Polymer Composites. *Prog. Polym. Sci.* **2010**, *35*, 1350–1375.

(9) Porwal, H.; Grasso, S.; Reece, M. J. Review of Graphene-Ceramic Matrix Composites. *Adv. Appl. Ceram.* **2013**, *112*, 443–454.

(10) Smeacetto, F.; Ferraris, M.; Salvo, M. Multilayer Coating with Self-Sealing Properties for Carbon–Carbon Composites. *Carbon* **2003**, *41*, 2105–2111.

(11) Pawlowski, L. Thermal Spray Techniques. In *The Science and Engineering of Thermal Spray Coatings*, 2nd ed.; John Wiley & Sons: Chichester, U.K., 2008; pp 67–113.

(12) Li, H.; Xie, Y.; Li, K.; Huang, L.; Huang, S.; Zhao, B.; Zheng, X. Microstructure and Wear Behavior of Graphene Nanosheets-Reinforced Zirconia Coating. *Ceram. Int.* **2014**, *40*, 12821–12829.

(13) Xie, Y.; Li, H.; Zhang, C.; Gu, X.; Zheng, X.; Huang, L. Graphene-Reinforced Calcium Silicate Coatings for Load-Bearing Implants. *Biomed. Mater.* **2014**, *9*, 025009.

(14) Liu, Y.; Dang, Z.; Wang, Y.; Huang, J.; Li, H. Hydroxyapatite/Graphene-Nanosheet Composite Coatings Deposited by Vacuum Cold Spraying for Biomedical Applications: Inherited Nanostructures and Enhanced Properties. *Carbon* **2014**, *67*, 250–259.

(15) García, E.; Nistal, A.; Martín de la Escalera, F.; Khalifa, A.; Sainz, M. A.; Osendi, M. I.; Miranzo, P. Thermally Sprayed Y_2O_3-Al_2O_3-SiO_2 Coatings for High Temperature Protection of SiC Ceramics. *J. Therm. Spray Technol.* **2015**, *24*, 185–193.

(16) Cao, X. Q.; Vassen, R.; Schwartz, S.; Jungen, W.; Tietz, F.; Stöever, D. Spray-Drying of Ceramics for Plasma-Spray Coating. *J. Eur. Ceram. Soc.* **2000**, *20*, 2433–2439.

(17) Cano, C.; Osendi, M. I.; Belmonte, M.; Miranzo, P. Effect of the Type of Flame on the Microstructure of CaZrO3 Combustion Flame Sprayed Coating. *Surf. Coat. Technol.* **2006**, *201*, 3307–3313.

DOI: 10.1021/acsami.5b02553
ACS Appl. Mater. Interfaces 2015, 7, 17656–17662

(18) Ferrari, A. C.; Meyer, J. C.; Scardaci, V.; Casiraghi, C.; Lazzeri, M.; Mauri, F.; Piscanec, S.; Jiang, D.; Novoselov, K. S.; Roth, S.; Geim, A. K. Raman Spectrum of Graphene and Graphene Layers. *Phys. Rev. Lett.* **2006**, *97*, 187401−187404.
(19) Kohli, J. T.; Condrate, R. A.; Shelby, J. R. Raman and Infrared Spectra of Rare Earth Aluminosilicate Glasses. *Phys. Chem. Glasses* **1993**, *34*, 81−88.
(20) Lee, T. Y. R. Thermal Diffusivity of Dispersed and Layered Composites. Ph.D. Thesis. Purdue University, West Lafeyette, IN, 1977.
(21) Miranzo, P.; García, E.; Ramírez, C.; González-Julián, J.; Belmonte, M.; Osendi, M. I. Anisotropic Thermal Conductivity of Silicon Nitride Ceramics Containing Carbon Nanostructures. *J. Eur. Ceram. Soc.* **2012**, *32*, 1847−1854.
(22) Kulkarni, A.; Wang, Z.; Nakamura, T.; Sampath, S.; Goland, A.; Herman, H.; Allen, J.; Ilavsky, J.; Long, G.; Frahm, J.; Steinbrech, R. W. Comprehensive Microstructural Characterization and Predictive Property Modeling of Plasma-Sprayed Zirconia Coatings. *Acta Mater.* **2003**, *51*, 2457−2475.
(23) Wang, Z.; Kulkarni, A.; Deshpande, S.; Nakamura; Herman, T. H. Effects of Pores and Interfaces on Effective Properties of Plasma Sprayed Zirconia Coatings. *Acta Mater.* **2003**, *51*, 5319−5334.
(24) Garcia, E.; Miranzo, P.; Soltani, R.; Coyle, T. W. Microstructure and Thermal Behavior of Thermal Barrier Coatings. *J. Therm. Spray Technol.* **2008**, *17*, 478−485.
(25) Young, J.; Crippen, R. Thermal Protection Systems, In *Wings in Orbit: Scientific and Engineering Legacies of the Space Shuttle, 1971−2010*; Hale, W., et al. Eds.; Government Printing Office: Washington DC, 2011; Vol. *3409*, pp 182−199.
(26) Ramirez, C.; Figueiredo, F.; Miranzo, P.; Poza, P.; Osendi, M. I. Graphene Nanoplatelet/Silicon Nitride Composites with High Electrical Conductivity. *Carbon* **2012**, *50*, 3607−3615.
(27) Ramírez, C.; Vega-Diaz, S. M.; Morelos-Gómez, A.; Figueiredo, F.; Terrones, M.; Osendi, M. I.; Belmonte, M.; Miranzo, P. Synthesis of Conducting Graphene/Si3N4 Composites by Spark Plasma Sintering. *Carbon* **2013**, *57*, 425−432.
(28) Watcharotone, S.; Dikin, D. A.; Stankovich, S.; Piner, R.; Jung, I.; Dommett, G. H. B.; Evmenenko, G.; Wu, S. E.; Chen, S. F.; Liu, C. P.; Nguyen, S. T.; Ruoff, R. S. Graphene-Silica Composite Thin Films as Transparent Conductors. *Nano Lett.* **2007**, *7*, 1888−1892.
(29) Fan, Y.; Wang, L.; Li, J.; Li, J.; Sun, S.; Chen, F.; Chen, L.; Jiang, W. Preparation and Electrical Properties of Graphene Nanosheet/Al_2O_3 Composites. *Carbon* **2010**, *48*, 1743−1749.
(30) Jankovsky, O.; Simek, P.; Sedmidubsky, D.; Huber, S.; Pumera, M.; Sofer, Z. Towards Highly Electrically Conductive and Thermally Insulating Graphene Nanocomposites: Al_2O_3 Graphene. *RSC Adv.* **2014**, *4*, 7418−7424.
(31) Miranzo, P.; Ramírez, C.; Román-Manso, B.; Garzón, L.; Gutiérrez, H. R.; Terrones, M.; Ocal, C.; Osendi, M. I.; Belmonte, M. In Situ Processing of Electrically Conducting Graphene/SiC Nanocomposites. *J. Eur. Ceram. Soc.* **2013**, *33*, 1665−1674.
(32) Román-Manso, B.; Domingues, E.; Figueiredo, F. M.; Belmonte, M.; Miranzo, P. Enhanced Electrical Conductivity of Silicon Carbide Ceramics by Addition of Graphene NanoPlatelets. *J. Eur. Ceram. Soc.* **2015**, *35*, 2723−2731.
(33) Fan, Y.; Jiang, W.; Kawasaki, A. Highly Conductive Few-Layer Graphene/Al_2O_3 Nanocomposites with Tunable Charge Carrier Type. *Adv. Funct. Mater.* **2012**, *22*, 3882−3889.
(34) Ramirez, C.; Miranzo, P.; Belmonte, M.; Osendi, M. I.; Poza, P.; Vega-Díaz, S. M.; Terrones, M. Extraordinary Toughening Enhancement and Flexural Strength in Si_3N_4 Composites Using Graphene Sheets. *J. Eur. Ceram. Soc.* **2014**, *34*, 161−169.
(35) Porwal, H.; Tatarko, P.; Grasso, S.; Hu, C.; Boccaccini, A. R.; Dlouhý, I.; Reece, M. J. Toughened and Machinable Glass Matrix Composites Reinforced with Graphene and Graphene-Oxide Nano Platelets. *Sci. Technol. Adv. Mater.* **2013**, *14*, 055007.
(36) Evans, A. G. The Mechanical Properties of Reinforced Ceramic, Metal and Intermetallic Matrix Composites. *Mater. Sci. Eng., A* **1991**, *143*, 63−76.
(37) Mesquita-Guimarães, J.; García, E.; Osendi, M. I.; Sevecek, O.; Bermejo, R. Effect of Aging on the Onset of Cracks due to Redistribution of Residual Stresses in Functionally Graded Environmental Barrier Coatings of mullite/ZrO_2. *Composites, Part B* **2014**, *61*, 199−205.
(38) García, E.; Mesquita-Guimarães, J.; Miranzo, P.; Osendi, M. I. Porous Mullite and Mullite-ZrO_2 Granules for Thermal Spraying Applications. *Surf. Coat. Technol.* **2011**, *205*, 4304−4311.
(39) García, E.; Mesquita-Guimarães, J.; Miranzo, P.; Osendi, M. I.; Wang, Y.; Lima, R. S.; Moreau, C. Mullite and Mullite/ZrO_2-7wt% Y_2O_3 Powders for Thermal Spraying of Environmental Barrier Coatings. *J. Therm. Spray Technol.* **2010**, *19*, 286−293.
(40) Nistal, A.; García, E.; García-Diego, C.; Osendi, M. I.; Miranzo, P. Flame Spraying of Adherent Si Coatings on SiC Substrates. *Surf. Coat. Technol.* **2015**, *270*, 8−15.
(41) Roine. A. *Outokumpu HSC Chemistry for Windows*, version 5.11; Outokumpu Research: Pori, Finland, 2002.
(42) Donaldson, A. B.; Taylor, R. E. Thermal Diffusivity Measurement by a Radial Heat Flow Method. *J. Appl. Phys.* **1975**, *46*, 4584−4589.
(43) Oliver, W. C.; Pharr, G. M. Improved Technique for Determining Hardness and Elastic Modulus Using Load and Displacement Sensing Indentation Experiments. *J. Mater. Res.* **1992**, *7*, 1564−1580.

DOI: 10.1021/acsami.5b02553
ACS Appl. Mater. Interfaces 2015, 7, 17656−17662